A one dimensional discrete approach for the determination of the cross sectional properties of composite rotor blades

Martín C. Saravia[*], L. Joaquín Saravia, Víctor H. Cortínez

Centro de Investigación en Mecánica Teórica y Aplicada, CONICET — Universidad Tecnológica Nacional, Facultad Regional Bahía Blanca, 11 de Abril 461, 8000 Bahía Blanca, Argentina

A R T I C L E   I N F O

A B S T R A C T

This work presents the theoretical aspects of a one dimensional computational approach for the determination of the cross sectional stiffness of composite rotor blades. The method is based on a vector variant of the classical lamination theory embedded into a geometrically exact large deformation-small strain thin-walled beam formulation, which is naturally oriented to multibody problems. The procedures rely on a one-dimensional discretization of the aerodynamic profile of the blade; this generates groups of finite segments of composite laminates which are assembled to find the stiffness properties of the blade cross section. The formulation accounts for warping and transverse shear; the warping problem is solved numerically by means of a one dimensional finite element formulation. The numerical tests show that the formulation gives very accurate results.

1. Introduction

Blades are the heart of wind turbines and helicopters; the dependency of the machine performance on its structural and aerodynamic behavior has turned the blade's structural design in a hot research subject. In large scale machines, composite materials are almost exclusively used; its superior fatigue characteristics, low weight-stiffness ratio, customizable deformation behavior and ability to fabricate complex geometries are the reasons behind this trend.

The continuously increasing size of modern rotors is modifying the design constraints; thus, to understand how these new scenario affects the performance and durability of the machines refined computational tools must evolve. Accurate computation of the mechanic behavior of modern blades requires not only advanced computational techniques but also new theoretical developments.

Two main difficulties arise while describing structural response of high aspect ratio blades: the accurate computation of its stiffness characteristics and the treatment of its finite deformation behavior. The complexity of both the material mapping and the cross sectional shape makes the task of computing the blade stiffness cumbersome; the problem complicates even more when the slenderness of the blade and the acting loads combine in such a way that finite deformations occur.

Computational modeling of composite blades continues to be investigated [1—6]. Although three dimensional modeling of the full composite blade is possible; the aeroelastic nature of the problem makes a full fluid-structure 3D simulation extremely computationally intensive, this opens the possibility for reduced theories. In this context, the beam approach have been extensively used in combination with 1D/2D aeroelastic codes to study the dynamic behavior of composite blades [5,7—12].

Thin walled beam theory is commonly used to describe the behavior of composite rotor blades [5,13—16]; often, contradictory conclusions about the capabilities of the theory to accurately model realistic composite blades were found. Several refinements of the classical thin-walled beam theory can be found in the literature [17—26], most of them claim that incorporation of new "effects" or "terms" in the motion equations leads to an overall improvement of the theory. Many of this conclusions are questionable and, as suggested in Ref. [15], some of these "improvements" are suspected to be the result of an incorrect implementation and/or an inconsistent formulation.

* Corresponding author.
E-mail address: msaravia@conicet.gov.ar (M.C. Saravia).

The use of a beam-like formulation necessarily implies the determination of the blade cross sectional stiffness matrix at various span locations; nowadays this task can be tackled through different methods: i) 3D shell modeling of the full blade with subsequent beam property extraction by static loading; it is an accurate procedure but it is also very time consuming [5,27], ii) 2D modeling of the cross section; it gives the most accurate results but the time required to model every stage of the blade is near the time required for 3D modeling [5,13,16,28]; and finally, iii) 1D modeling of the cross section by thin-walled beam theory; it gives good results with minimal time consumption.

Nowadays, the one dimensional approach is widely used in rotor blade design. Chen et al. [13] presented a detailed assessment of the most used computational tools for calculating wind turbine blade cross sectional stiffness. The study included numerical comparisons between: analytic results, the 2D solid approach VABS, developed by Prof. Hodges and coworkers [16,28,29] and the 1D cross sectional analysis tools: FAROB [30], developed at the Dutch Knowledge Center of Wind Energy Materials and Construction; PreComp [31], developed at National Renewable Energy Laboratory and CROSTAB [32], developed at the Energy Research Center of the Netherlands. The study concludes that the 1D approaches are inconsistent and therefore its applicability to modeling realistic blades is questionable; one of the objectives of this paper is to show that this statement is not correct.

Resor et al. [33] compared results obtained with PreComp and BPE, a 3D shell approach developed by Global Energy Concepts and Sandia National Laboratories [34], to those obtained in experimental testing of the BSDS blade; according to this paper the overall difference between PreComp and BPE is in the range of 15–25% and the difference between the experimental results and BPE are in the range of 5–20%. In a later study, Resor and Paquette also included VABS in the assessment of the cross sectional stiffness calculation [35]. The paper reproduced the same results of [13] for a particular wind turbine cross section, only diagonal terms of the stiffness matrix were presented. For a CX-100 blade, discrepancies were found between VABS and BPE, especially in sections near the blade's root, this was attributed to local straining.

More recently, Wang et al. [8] presented a 1D approach based on the classical lamination theory and Bredt-Batho shear flow. The developments were implemented in a Matlab code called CBCSA, the code was compared against PreComp and all reported differences were surprisingly below 0.1%, excepting for the torsional stiffness where the difference was up to 46%. Conclusions of this paper state that CBCSA has higher accuracy than PreComp in the prediction of the torsional stiffness; no coupling terms was presented in the paper.

In the present paper a 1D formulation for calculating the cross sectional properties of composite blades is presented. The approach permits to model generally anisotropic materials and arbitrary geometries, the latter implies unlimited number of shear webs as well as arbitrary thickness distribution. The formulation is based on a discrete implementation of the classical lamination theory (CLT) and a large deformation-small strain thin-walled beam formulation, which is naturally oriented to multibody problems. Only the wing profile of the blade is needed as geometrical input; this profile is discretized in groups of segments to which material and lamination properties are assigned. The formulation corrects the torsional problem by including at the constitutive level the effects of warping; the warping function is calculated numerically by means of a finite element approach without requiring an additional input. The formulation is implemented in a computational code and several numerical test are performed in order to assess accuracy; results show an excellent agreement with those of an accurate 2D approach.

2. The blade geometric model

2.1. A realistic blade

The cross sectional shape of modern blades is imposed by the aerodynamic design, wing profiles and chord lengths constraint the blade outer shape. Aerodynamic and inertia loads are the inputs of the structural design of the blade, which is mainly focused on the definition of the position and number of shear webs, the lamination stacking sequence and the material mapping. Buckling and fatigue are commonly the primary concerns.

A modern approach for the determination of the blade structural performance must contain theoretical developments and computational procedures conceived to model *realistic blades*. The nonlinear nature of the aeroelastic environment in which the blade works makes difficult a conscious assessment of the impact of geometrical and material simplifications on the accuracy of the computational prediction of its response.

A realistic structural blade model based on beam theory should capture accurately its 3D dynamic behavior; it also must be capable of predicting a reasonable stress distribution along the blade span. This requirements imply a good prediction of the cross sectional stiffness parameters. The material mapping on a modern blade is complex, from the outermost to the innermost surfaces a realistic model should include the following materials:

- Gelcoat: a smooth surface coating to enhance aerodynamic performance.
- Nexus: a soft absorbent layer of material to facilitate gelcoat painting.
- Double-bias composite: 45° oriented unidirectional plies of glass fiber, carbon fiber, Kevlar, etc., used to improve torsional stiffness.
- Core Material: very light material to be used as fill at selected locations in order to increase local inertia of the blade and thus avoid local buckling, typically materials are: balsa, foam and honeycomb.
- Unidirectional ply: composite material with high axial stiffness in order to give flexural strength to the blade.

Many modern designs incorporate a box-spar with variable shape along the blade span. The box-spar is the structural heart of the blade, typically it is rectangular shaped and its material mapping is double bias plus unidirectional composite; spar caps are normally built with unidirectional fibers or even rovings while shear webs require biax and/or triax laminates. The unidirectional fibers provide most of the tensile and flexural strength; they run from the blade's tip to its root through the box-spar, around the mounting bushings and back out the root. In many cases, the double-bias and unidirectional plies are interspersed to form a single laminate. The interior of the box-spar consists of an embedded core material to prevent buckling.

2.2. 1D blade model

It has been said that wind turbine and helicopter rotor blades are wing shaped slender elements for which the cross sectional shapes are imposed by aerodynamic requirements [2,4]. With the outer surface a priori defined, the structural design implies the definition of the stacking sequence of composite material layers to be placed in the interior of the blade such as to satisfy durability and functionality requirements.

The blade wing profile is given as a set of planar points in an ASCII table; the present approach uses this points to define lines that will be split or joined in segments according to a desired target

density, see Fig. 1. The process of generating a one dimensional mesh of straight segments is the starting step of the formulation (Fig. 2).

To each segment a composite material and a lamination sequence is assigned. The stacking sequence starts in the outer contour of the cross section and directs inward following the direction of the corresponding segment normal.

3. Kinematics

3.1. Coordinate systems and transformations

From the computational point of view, the cross sectional stiffness parameters of the blade are not only a function of its geometrical and material data but also of the strain measure chosen to describe its mechanics. As a consequence, a particular cross sectional stiffness measure is strictly consistent only with the kinematic formulation from which it was derived.

In order to evaluate the strain state of the blade, three frames of reference attached to the cross section are introduced:

a) a reference material frame $\{E_1, E_2, E_3\}$, its origin is set anywhere inside the closed curved defined by the wing profile.
b) a sectional frame $\{E_1, \widehat{n}, \widehat{s}\}$ which is taken as the trihedron of the mid-contour curve, this system is arc length parameterized, $\widehat{s}$ is anticlockwise tangent to the contour unit vector, $\widehat{n}$ is the outward normal unit vector and E_1 is the axial unit vector, which coincides with the binormal. The origin of the coordinate system is set at the segment midpoint.
c) a layer individual frame $\{\widehat{1}, \widehat{2}, \widehat{3}\}$, for which the direction $\widehat{2}$ is the direction of the normal, i. e. $\widehat{n}$, and the direction $\widehat{1}$ is oriented to coincide with some distinct direction of the lamina.

The derivations that will be presented hereafter require the use of frame transformations; the constitutive equations of the at some point need to be expressed in the sectional frame, also stress and strain measures in the sectional frame will be transformed to the reference frame. The transformation tensor that allows transforming vectors in the reference frame to the sectional frame is given by

$$Q_s = \begin{bmatrix} E_1^T & \widehat{n}^T & \widehat{s}^T \end{bmatrix}. \tag{1}$$

In the same way, the transformations from the layer frame to the sectional are done through a vector variant of a frame transformation, for brevity it is not shown here but the reader can refer to [36,37] if additional details are needed.

3.2. Kinematic description

The so called cross sectional stiffness is the relation between one dimensional strain measures and its conjugate forces. Since the strain measures depend on the derivatives of the blade configuration, the stress−strain relations are affected by the kinematic definitions, and then the stiffness of the blade is a function of the kinematic assumptions.
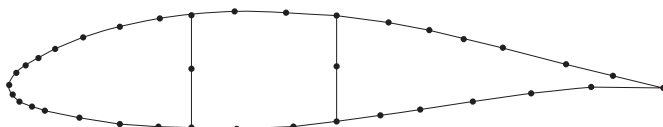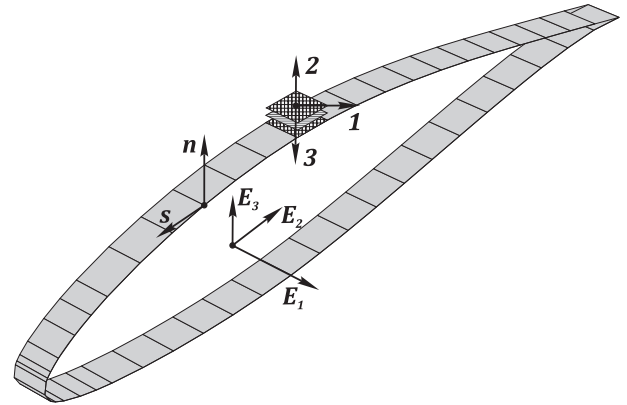

Fig. 2. Blade reference systems.

It is assumed that the blade is moderately slender; that is: its mechanic behavior can be reasonably approximated by beam theory, i.e. it is formed by a group of cross sections that follow the hypotheses:

a) *they can undergo finite displacements and finite rotations.*
b) *they behave as rigid in their own planes.*
c) *they are free to warp out of their planes.*
d) *the warping elastic energy is small.*
e) *they are built with anisotropic materials.*
f) *strains are small.*

The locus of cross sectional mass centroids is called the *reference line of the beam* (denoted as $\mathscr{C}$). The kinematic description of the blade is written from the relations between two states, an undeformed reference state (denoted as $\mathscr{B}_0$) and a deformed state (denoted as $\mathscr{B}$), as it is shown in Fig. 3. Being a_i a spatial frame of reference and E_i the reference configuration frame, a current frame e_i attached to the cross section is defined to express clearly the kinetic relations.

The position change of a point in the deformed state measured with respect to the undeformed reference state can be expressed in the global coordinate system a_i in terms of a displacement vector $u=(u_1, u_2, u_3)$.

The current frame e_i is a function of a running length coordinate along the reference line of the blade, denoted as x. The origin of e_i is

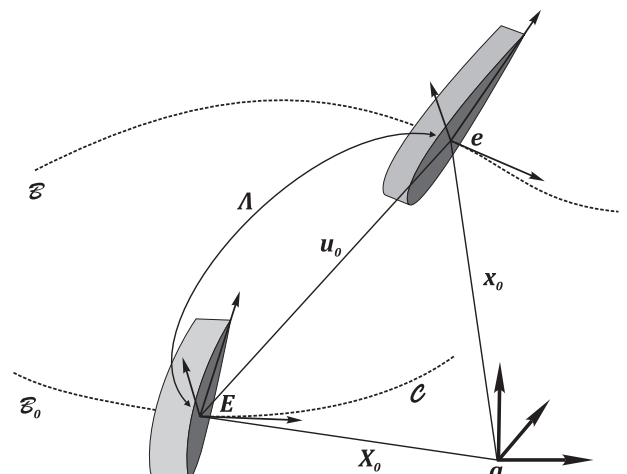**Fig. 1.** Segment division of a typical blade cross section.

Fig. 3. Blade kinematics.

located on the reference line of the blade and is called *pole*. The cross-section of the blade but is initially normal to the reference line.

The relations between the orthonormal frames are given by the transformations:

$$\boldsymbol{E}_i = \Lambda_0(x)\boldsymbol{a}_i, \quad \boldsymbol{e}_i = \Lambda(x)\boldsymbol{E}_i, \tag{2}$$

where $\Lambda_0(x)$ and $\Lambda(x)$ are two-point tensor fields $\in SO(3)$, the special orthogonal (Lie) group. Thus, it is satisfied that $\Lambda_0^T\Lambda_0 = \boldsymbol{I}, \Lambda^T\Lambda = \boldsymbol{I}$. It is considered that the blade span can be modeled by a set of straight elements, so $\Lambda_0 = \boldsymbol{I}$.

Recalling the relations (2), the position vectors of a point in the undeformed and deformed configurations respectively can be expressed as:

$$\boldsymbol{X}(x, \xi_2, \xi_3) = \boldsymbol{X}_0(x) + \sum_{i=2}^{3} \xi_i \boldsymbol{E}_i,$$
$$\boldsymbol{x}(x, \xi_2, \xi_3, t) = \boldsymbol{x}_0(x, t) + \sum_{i=2}^{3} \xi_i \boldsymbol{e}_i + \omega \; \boldsymbol{e}_1, \tag{3}$$

where in both equations the first term stands for the position of the pole and the second term stands for the position of a point within the cross section relative to the pole; the coordinates ξ_2 and ξ_3 are the components of the position vector of a point in the cross section expressed in Ref. $\boldsymbol{E}_i$. The variable ω accounts for the displacements in the cross section due to torsional warping.

Now, the hypothesis *d)* can be invoked, and thus ω can be excluded from Eq. (3) before the evaluation of the strain state of the blade. Although it is proposed to disregard the warping displacement at the kinematic level, cross sectional warping shall be recalled at the constitutive level to account for its effect on the torsional flexibility. This point is important and will be clarified later.

At this point it is possible to express the displacement field as:

$$\boldsymbol{U}(x, \xi_2, \xi_3, t) = \boldsymbol{x} - \boldsymbol{X} = \boldsymbol{u}(x, t) + (\Lambda - \boldsymbol{I})\sum_{2}^{3} \xi_i \boldsymbol{E}_i, \tag{4}$$

where $\boldsymbol{u}$ represents the displacement of the kinematic center of reduction, i.e. the pole. The nonlinear manifold of 3D rotation transformations $\Lambda(\boldsymbol{\theta})$ (belonging to the special orthogonal Lie Group SO(3)) is described mathematically via the exponential map

$$\Lambda(\boldsymbol{\theta}) = \cos\theta \boldsymbol{I} + \frac{\sin\theta}{\theta}\boldsymbol{\Theta} + \frac{1-\cos\theta}{\theta^2}\boldsymbol{\theta}\otimes\boldsymbol{\theta}, \tag{5}$$

where $\boldsymbol{\theta} = [\theta_1 \; \theta_2 \; \theta_3]^T$ is the rotation vector, θ its modulus and $\boldsymbol{\Theta}$ is its skew symmetric matrix. The set of kinematic variables is then formed by three displacements and three rotations as:

$$\mathcal{V} := \left\{ \boldsymbol{\phi} = [\boldsymbol{u}, \boldsymbol{\theta}]^T : [0, \ell] \to R^3 \right\},$$
$$[\boldsymbol{u}, \boldsymbol{\theta}]^T = [u_1, u_2, u_3, \theta_1, \theta_2, \theta_3]^T. \tag{6}$$

Note that since no constraint has been imposed to the orientation of $\boldsymbol{e}_i$, generally $\boldsymbol{e}_1 \cdot \boldsymbol{x}_{,1} \neq 0$ and thus transverse shear is permitted.

3.3. The small Green–Lagrange strain measure (SGS)

The cross sectional strain measures are obtained from the kinematic assumptions of the blade; it is shown in Ref. [38] that under the *a/f* assumptions of Section 2 the small Green–Lagrange strain measure is an excellent choice to describe a large

deformation-small strain behavior. Although the kinematic behavior of the blade allows large deformations, the constitutive law of anisotropic materials is only valid for Small strains, and thus for a consistent derivation of the equilibrium equations the use of a small strain measure is sufficient.

Since blades experiment deformation plus rigid body motion, the strain measures must be objective. It was shown in Ref. [38] that assuming small strains has no consequence in the capability of the large deformation-small strain theory to describe the dynamic response of a beam under this scenario. Moreover, the computational implementation simplifies considerably, so this is the approach that will be followed in this paper. For the sake of brevity only minor details of the derivation of the SGS measure are going to be presented here; for more information the reader should refer to [38].

The Green–Lagrange strain tensor is defined as a function of the deformation gradient $\boldsymbol{F}$ as

$$\boldsymbol{E} = \frac{1}{2}\left(\boldsymbol{F}^T\boldsymbol{F} - \boldsymbol{I}\right); \tag{7}$$

this expression measures arbitrary straining. It was shown in Ref. [38] that under the kinematic hypotheses *a/f* the deformation gradient has de following expression

$$\boldsymbol{F} = \Lambda + \left(\boldsymbol{x}_0' - \boldsymbol{e}_1 + \xi_\alpha \boldsymbol{e}_\alpha'\right)\otimes \boldsymbol{E}_1, \tag{8}$$

where $\xi_\alpha / \alpha = 1, 2$ are the components of the position vector a point in the cross section relative to the section pole, in the reference configuration $\boldsymbol{r} = \xi_2 \boldsymbol{E}_2 + \xi_3 \boldsymbol{E}_3$.

Now, defining the pure current strain vector

$$\boldsymbol{\varepsilon} = \boldsymbol{x}_0' - \boldsymbol{e}_1 + \xi_\alpha \boldsymbol{e}_\alpha', \tag{9}$$

where the index $\alpha = 2, 3$, the deformation gradient can be written in compact form as

$$\boldsymbol{F} = \Lambda + \boldsymbol{\varepsilon}\otimes\boldsymbol{E}_1. \tag{10}$$

This expression can be injected into Eq. (7) and after dropping the nonlinear pure strain term it is straightforward to obtain the SGS tensor

$$\boldsymbol{E} = \frac{1}{2}\begin{bmatrix} 2\boldsymbol{\varepsilon}\cdot\boldsymbol{e}_1 & \boldsymbol{\varepsilon}\cdot\boldsymbol{e}_2 & \boldsymbol{\varepsilon}\cdot\boldsymbol{e}_3 \\ \boldsymbol{\varepsilon}\cdot\boldsymbol{e}_2 & 0 & 0 \\ \boldsymbol{\varepsilon}\cdot\boldsymbol{e}_3 & 0 & 0 \end{bmatrix}. \tag{11}$$

The SGS tensor can now be written in vector form as

$$\boldsymbol{e} = \begin{bmatrix} \boldsymbol{x}_0'\cdot\boldsymbol{e}_1 - 1 + \xi_\alpha\boldsymbol{e}_\alpha'\cdot\boldsymbol{e}_1 \\ \boldsymbol{x}_0'\cdot\boldsymbol{e}_2 + \xi_3\boldsymbol{e}_3'\cdot\boldsymbol{e}_2 \\ \boldsymbol{x}_0'\cdot\boldsymbol{e}_3 + \xi_2\boldsymbol{e}_2'\cdot\boldsymbol{e}_3 \end{bmatrix}. \tag{12}$$

The three components of the SGS vector are: a normal strain in the direction of reference line of the blade and two shear strains. All three components are formed by two terms, a constant term (which is not a function of the location of the point in the cross section) and a linear term.

The SGS vector can be re-written in matrix form as

$$\boldsymbol{e} = \boldsymbol{D}\,\boldsymbol{\varepsilon}, \tag{13}$$

being $\boldsymbol{D}$ a cross sectional matrix such that

$$D = \begin{bmatrix} E_1 & r \\ E_2 & r \times E_2 \\ E_3 & r \times E_3 \end{bmatrix} = \begin{bmatrix} 1 & 0 & 0 & 0 & \xi_2 & \xi_3 \\ 0 & 1 & 0 & -\xi_3 & 0 & 0 \\ 0 & 0 & 1 & \xi_2 & 0 & 0 \end{bmatrix}, \tag{14}$$

and ε the so called generalized strain vector

$$\varepsilon = \begin{bmatrix} x_0' \cdot e_1 - 1 \\ x_0' \cdot e_2 \\ x_0' \cdot e_3 \\ e_2' \cdot e_3 \\ e_2' \cdot e_1 \\ e_3' \cdot e_1 \end{bmatrix}. \tag{15}$$

For convenience and without implying a simplification it has been assumed that $E_i = a_i$.

At last, curvature and axial-shear strain vectors are defined for future use as

$$\gamma = \begin{bmatrix} \varepsilon & \gamma_2 & \gamma_3 \end{bmatrix}^T = \begin{bmatrix} x_0' \cdot e_1 - 1 & x_0' \cdot e_2 & x_0' \cdot e_3 \end{bmatrix}^T,$$
$$\kappa = \begin{bmatrix} \kappa_1 & \kappa_2 & \kappa_3 \end{bmatrix}^T = \begin{bmatrix} e_2' \cdot e_3 & e_2' \cdot e_1 & e_3' \cdot e_1 \end{bmatrix}^T. \tag{16}$$

Then a very convenient form of the generalized strain vector can be written in the form

$$\varepsilon = \begin{bmatrix} \gamma^T & \kappa^T \end{bmatrix}^T. \tag{17}$$

3.4. The sectional strain measures

The SGS vector expresses the strain state of the blade in the reference frame. In order to write the constitutive equations and make hypotheses about the sectional behavior it is necessary to express the SGS in the cross sectional frame $\{E_1, \hat{n}, \hat{s}\}$.

Recall that the origin of the cross sectional system is placed half a thickness inward from the outer contour and moves along the cross section contour in anticlockwise direction; then, the tangent unit vector can be found as the derivative of the mid-contour position vector $\bar{r} = \bar{\xi}_2 E_2 + \bar{\xi}_3 E_3$. This is

$$\hat{s} = \frac{d\bar{r}}{ds} = \bar{\xi}_2' E_2 + \bar{\xi}_3' E_3, \tag{18}$$

where $\bar{\xi}_i'$ represents derivatives of mid-contour cross sectional coordinates with respect to s. The normal unit vector can be obtained invoking the orthogonality condition of the coordinate system, then

$$\hat{n} = \hat{s} \times E_1 = \bar{\xi}_3' E_2 - \bar{\xi}_2' E_3. \tag{19}$$

The position vector of a point in the cross section expressed in the sectional coordinate system is

$$r_s = (\bar{r}_n + n)\hat{n} + \bar{r}_s \hat{s},$$
$$\bar{r}_s = \bar{r}_n \hat{n} + \bar{r}_s \hat{s}, \tag{20}$$

where the mid-contour components $\bar{r}_i$ are obtained as

$$\bar{r}_n = \bar{r}_s \cdot \hat{n} = \xi_2 \bar{\xi}_3' - \xi_3 \bar{\xi}_2',$$
$$\bar{r}_s = \bar{r}_s \cdot \hat{s} = \xi_2 \bar{\xi}_2' + \xi_3 \bar{\xi}_3'. \tag{21}$$

Another relation that is needed is the position of a point in the cross section as a function of the mid-contour coordinates, this is

$$r = \bar{r} + n\hat{n} = \left(\bar{\xi}_2 + n\bar{\xi}_3'\right)E_2 + \left(\bar{\xi}_3 - n\bar{\xi}_2'\right)E_3. \tag{22}$$

The sectional frame transformation tensor operates over the SGS tensor to give the strains in the sectional system as

$$e = Q_s^T E Q_s; \tag{23}$$

making explicit its vector form one obtains

$$e = \begin{bmatrix} \varepsilon_x \\ \gamma_{xs} \\ \gamma_{xn} \end{bmatrix} = \begin{bmatrix} \varepsilon + \xi_2 \kappa_2 + \xi_3 \kappa_3 \\ \bar{\xi}_2' \gamma_2 + \bar{\xi}_3' \gamma_3 + \left(\xi_2 \bar{\xi}_3' - \xi_3 \bar{\xi}_2'\right)\kappa_1 \\ \bar{\xi}_3' \gamma_2 - \bar{\xi}_2' \gamma_3 - \left(\xi_2 \bar{\xi}_2' + \xi_3 \bar{\xi}_3'\right)\kappa_1 \end{bmatrix}; \tag{24}$$

From the above expression it is seen that expanding the terms ξ_i it is obtained

$$e = \begin{bmatrix} \varepsilon + \left(\bar{\xi}_2 + n\bar{\xi}_3'\right)\kappa_2 + \left(\bar{\xi}_3 - n\bar{\xi}_2'\right)\kappa_3 \\ \bar{\xi}_2' \gamma_2 + \bar{\xi}_3' \gamma_3 + \left(\left(\bar{\xi}_2 + n\bar{\xi}_3'\right)\bar{\xi}_3' - \left(\bar{\xi}_3 - n\bar{\xi}_2'\right)\bar{\xi}_2'\right)\kappa_1 \\ \bar{\xi}_3' \gamma_2 - \bar{\xi}_2' \gamma_3 - \left(\left(\bar{\xi}_2 + n\bar{\xi}_3'\right)\bar{\xi}_2' + \left(\bar{\xi}_3 - n\bar{\xi}_2'\right)\bar{\xi}_3'\right)\kappa_1 \end{bmatrix}. \tag{25}$$

Now, arranging some terms in the last equation and using Eq. (21), the following clear expression for the SGS expressed in the sectional frame is found

$$e_s = \begin{bmatrix} \varepsilon_x \\ \gamma_{xs} \\ \gamma_{xn} \end{bmatrix} = \begin{bmatrix} \varepsilon + \left(\kappa_3 \bar{\xi}_2 + \kappa_2 \bar{\xi}_3\right) + n\left(\kappa_3 \bar{\xi}_3' - \kappa_2 \bar{\xi}_2'\right) \\ \left(\bar{\xi}_2' \gamma_2 + \bar{\xi}_3' \gamma_3\right) + \kappa_1 r_n \\ \left(\bar{\xi}_3' \gamma_2 - \bar{\xi}_2' \gamma_3\right) - \kappa_1 \bar{r}_s \end{bmatrix}, \tag{26}$$

The last equation can be written as a function of the generalized strains as

$$e_s = D_s \varepsilon = \begin{bmatrix} 1 & r \\ \hat{s} & r_n 1 \\ \hat{n} & -\bar{r}_s 1 \end{bmatrix} \begin{bmatrix} \gamma \\ \kappa \end{bmatrix} \tag{27}$$

where $r_n = \bar{r}_n + n$. For convenience, it has been assumed that $E_1 = 1 = \{1,0,0\}$.

The explicit form of D_s reads

$$D_s = \begin{bmatrix} 1 & 0 & 0 & 0 & \bar{\xi}_3 - n\bar{\xi}_2' & \bar{\xi}_2 + n\bar{\xi}_3' \\ 0 & \bar{\xi}_2' & \bar{\xi}_3' & r_n & 0 & 0 \\ 0 & \bar{\xi}_3' & -\bar{\xi}_2' & -\bar{r}_s & 0 & 0 \end{bmatrix}, \tag{28}$$

4. Composite material modeling

4.1. Constitutive relations

The derivation of the constitutive relations of composite materials is straightforward; however, the various hypotheses that can be used lead to the emergence of a wide range of formulations [15,20]. This paper aims to show that, for the target application, the simplest constitutive formulation can give accurate results.

To derive the constitutive equations, the layer frame of reference $\{\hat{1}, \hat{2}, \hat{3}\}$ is be used. Every layer of composite material is assumed to lie in the $\{E_1, \hat{s}\}$ plane and thus the normal direction $\hat{n}$ of the sectional frame is coincident with $\hat{2}$ in the layer frame.

From heron it is assumed that every layer is orthotropic, so the constitutive equations can be written as

$$\begin{bmatrix} \sigma_1 \\ \sigma_2 \\ \sigma_3 \\ \sigma_{23} \\ \sigma_{31} \\ \sigma_{12} \end{bmatrix} = \begin{bmatrix} C_{11} & C_{12} & C_{13} & 0 & 0 & 0 \\ C_{12} & C_{22} & C_{23} & 0 & 0 & 0 \\ C_{13} & C_{23} & C_{33} & 0 & 0 & 0 \\ 0 & 0 & 0 & C_{44} & 0 & 0 \\ 0 & 0 & 0 & 0 & C_{55} & 0 \\ 0 & 0 & 0 & 0 & 0 & C_{66} \end{bmatrix} \begin{bmatrix} \varepsilon_1 \\ \varepsilon_2 \\ \varepsilon_3 \\ \gamma_{23} \\ \gamma_{31} \\ \gamma_{12} \end{bmatrix}. \qquad (29)$$

Now, invocation of the kinematic constraints imposed by the hypotheses in Section 3 would require to set $\varepsilon_2=\gamma_{23}=\gamma_{12}=0$; this is consistent with the kinematical hypotheses but it results in an overestimation of the blade cross section stiffness [36]. On the other hand, the plane stress assumption is by nature inconsistent with the kinematical hypothesis b) (the SGS tensor has three no null independent components and the plane stress state gives a full tensor, this is a known incompatibility of thin-walled beam formulations).

In virtue of the above comment, in this paper it is chosen to maintain the "plane stress inconsistency" because the plane stress assumption is much more representative of the true cross sectional stress state than that obtained using a consistent zero strain approach.

After inversion of Eq. (29) it is possible to set $\sigma_2=\sigma_{23}=\sigma_{12}=0$, this allows to eliminate the full rows and columns of the corresponding indexes and obtain the flexibility matrix

$$\begin{bmatrix} \varepsilon_1 \\ \varepsilon_3 \\ \gamma_{13} \end{bmatrix} = \begin{bmatrix} S_{11} & S_{13} & 0 \\ S_{13} & S_{33} & 0 \\ 0 & 0 & S_{55} \end{bmatrix} \begin{bmatrix} \sigma_1 \\ \sigma_3 \\ \sigma_{13} \end{bmatrix} \qquad (30)$$

The last expression can be transformed to the sectional frame, then the following compliance equation is obtained

$$\begin{bmatrix} \varepsilon_x \\ \varepsilon_s \\ \gamma_{xs} \end{bmatrix} = \begin{bmatrix} Q_{11} & Q_{12} & Q_{13} \\ & Q_{22} & Q_{23} \\ & & Q_{33} \end{bmatrix} \begin{bmatrix} \sigma_x \\ \sigma_s \\ \tau_{xs} \end{bmatrix} \qquad (31)$$

Invoking the kinematic hypothesis c) of Section 3.2 it is possible to set $\varepsilon_s=0$, then the compliance equations could be corrected accordingly, but it is well known that for composite beams the assumption $\varepsilon_s=0$ leads to an overstiffening that can render the theory useless [15,20,36]. Again, it is chosen to use the inconsistent hypothesis $\sigma_s=0$, which leads to the following constitutive equation

$$\begin{bmatrix} \varepsilon_x \\ \gamma_{xs} \end{bmatrix} = \begin{bmatrix} Q_{11} & Q_{13} \\ Q_{13} & Q_{33} \end{bmatrix} \begin{bmatrix} \sigma_x \\ \tau_{xs} \end{bmatrix} \qquad (32)$$

Inversion gives:

$$\begin{bmatrix} \sigma_x \\ \tau_{xs} \end{bmatrix} = \begin{bmatrix} A_{11} & A_{13} \\ A_{13} & A_{33} \end{bmatrix} \begin{bmatrix} \varepsilon_x \\ \gamma_{xs} \end{bmatrix} \qquad (33)$$

Recalling Eq. (27) the constitutive equations can be expressed in matrix form as

$$\boldsymbol{\sigma}_s = \boldsymbol{C}\boldsymbol{D}_s\boldsymbol{\varepsilon} \qquad (34)$$

where

$$\boldsymbol{\sigma} = \begin{bmatrix} \sigma_x \\ \tau_{xs} \end{bmatrix}, \quad \boldsymbol{C} = \begin{bmatrix} A_{11} & A_{13} \\ A_{13} & A_{33} \end{bmatrix}, \quad \boldsymbol{D}_s = \begin{bmatrix} \mathbf{1} & \boldsymbol{r} \\ \widehat{\boldsymbol{s}} & r_n\mathbf{1} \end{bmatrix} \qquad (35)$$

Expression (34) is the constitutive equation that will be used for the calculation of the cross sectional properties of the composite blade; note that this could be considered equivalent to the uniaxial stress equation.

4.2. Warping correction

Up to this point the formulation does not include the effect of warping, this is because it has been assumed in Section 3.2 that the warping elastic energy is negligible; however, if torsional problem is not corrected to allow out of plane warping, the torsional stiffness is wrongly predicted. It is known that the correction of the torsional problem via calculation of the torsional shear flow using for example the Bredt-Batho is far from straightforward when the cross section is multi-celled [15,20]; this is the case of wind turbine cross sections, so devising a new approach where the correct torsional stiffness can be obtained independently of the number of cells in the cross section is greatly desired.

Isolating the torsional problem, the axial equilibrium equation of the beam under the current hypotheses is given by

$$\begin{aligned} \nabla \cdot \boldsymbol{\tau} &= 0, \\ \boldsymbol{\tau} &= \tau_{xn}\widehat{\boldsymbol{n}} + \tau_{xs}\widehat{\boldsymbol{s}}. \end{aligned} \qquad (36)$$

The boundary condition is

$$\boldsymbol{\tau} \cdot \widehat{\boldsymbol{n}} = \tau_{xn} = 0 \quad in \ S_1 \cup S_2, \qquad (37)$$

where S_1 and S_2 are of the outer and inner contours respectively.

Now, it is assumed that the displacement field due to torsion is given by

$$\boldsymbol{u}_t = \frac{d\psi}{dx}\omega\boldsymbol{E}_1 + \psi r_s\widehat{\boldsymbol{n}} + \psi r_n\widehat{\boldsymbol{s}}, \qquad (38)$$

where ψ is a variable that accounts for the torsional twist.

The shear stresses in the blade section are given by

$$\begin{aligned} \tau_{xn} &= G_{xn}\gamma_{xn} = G_{xn}\left(\frac{\partial u_x}{\partial n} + \frac{\partial u_n}{\partial x}\right), \\ \tau_{xs} &= G_{xs}\gamma_{xs} = G_{xs}\left(\frac{\partial u_x}{\partial s} + \frac{\partial u_s}{\partial x}\right). \end{aligned} \qquad (39)$$

Injecting Eq. (38) into the above expression yields

$$\begin{aligned} \gamma_{xn} &= \frac{d\psi}{dx}\left(\frac{\partial\omega}{\partial n} + r_s\right), \\ \gamma_{xs} &= \frac{d\psi}{dx}\left(\frac{\partial\omega}{\partial s} + r_n\right). \end{aligned} \qquad (40)$$

which gives

$$\boldsymbol{\tau} = G_{xn}\frac{d\psi}{dx}\left(\frac{\partial\omega}{\partial n} + r_s\right)\widehat{\boldsymbol{n}} + G_{xs}\frac{d\psi}{dx}\left(\frac{\partial\omega}{\partial s} + r_n\right)\widehat{\boldsymbol{s}} \qquad (41)$$

Recalling the constitutive Eq. (34) and assuming that for small torsional twist

$$\frac{d\psi}{dx} \cong \boldsymbol{e}_2' \cdot \boldsymbol{e}_3, \qquad (42)$$

consideration of for the warping effect at the constitutive level requires a minimal modification of the constitutive equations. So, definition of the cross sectional matrix $\boldsymbol{D}_s$ as

$$\boldsymbol{D}_s = \begin{bmatrix} \mathbf{1} & \boldsymbol{r} \\ \widehat{\boldsymbol{s}} & (r_n + \omega_s')\mathbf{1} \end{bmatrix}, \qquad (43)$$

where ω_s' is the derivative of the out of plane warping function respect to the running length coordinate. It must be noted that some high order terms have been dropped.

Analytical obtention of the warping function of a blade cross section is not possible because not only it is very difficult to obtain a function that can describe the wing shape but also this function would surely be non-smooth. Then, it is required to draw on a numerical method to obtain it.

The weak form of the axial equilibrium Eq. (36) is obtained by weighting the equilibrium equation with the axial displacement and integrating as

$$\int_A (\nabla \cdot \boldsymbol{\tau}) \delta u_{\boldsymbol{E}_1} \ dA = 0, \tag{44}$$

where $u_{\boldsymbol{E}_1}$ is the axial displacement and A is the cross sectional area.

Application of Gauss's theorem together with the boundary condition (37) yields

$$\int_A \nabla \delta u_{\boldsymbol{E}_1} \cdot \boldsymbol{\tau} dA = 0. \tag{45}$$

Assuming $\omega = f(s)$ the gradient has only one non-zero component

$$\nabla \delta u_{\boldsymbol{E}_1} = \frac{d\psi}{dx} \delta \omega_s'. \tag{46}$$

This permits to write the weak equilibrium Eq. (44) as

$$\int_A \delta \omega_s' G_{xs} \left(\omega_s' + r_n \right) dA = 0; \tag{47}$$

here the first term is the system stiffness and the second term is the system force.

Integration over the mid-contour S is performed in the sectional frame; after integrating in $\widehat{\boldsymbol{n}}$ it is obtained

$$\Delta n G_{xs} \int_S \delta \omega_s' \ \omega_s' \ ds + G_{xs} \int_S \delta \omega_s' \left(\bar{r}_n \Delta n + \frac{n^2}{2} \Big|_{n_1}^{n_2} \right) ds = 0. \tag{48}$$

In order to solve the above equations, the geometric data from the discretized cross section is used to formulate a 1D finite element; the warping function can be interpolated using linear shape functions as

$$\omega = \boldsymbol{N}_\omega \widehat{\boldsymbol{\omega}}, \\ \boldsymbol{N}_\omega = [\, N_1 \quad N_2 \,], \quad \widehat{\boldsymbol{\omega}} = \begin{bmatrix} \widehat{\omega}_1 \\ \widehat{\omega}_2 \end{bmatrix}. \tag{49}$$

where $\widehat{\omega}_i$ are nodal values of the warping function.

The discrete version of the warping equilibrium Eq. (48) can be written as

$$\Delta n \, \delta \widehat{\boldsymbol{\omega}}^T \left(\int_S G_{xs} \boldsymbol{N}_\omega'^T \boldsymbol{N}_\omega' \ ds \right) \widehat{\boldsymbol{\omega}} \\ + \delta \widehat{\boldsymbol{\omega}}^T \left(\int_S G_{xs} \boldsymbol{N}_\omega'^T \left(\bar{r}_n \Delta n + \frac{n^2}{2} \Big|_{n_1}^{n_2} \right) ds \right) = 0, \tag{50}$$

which can be expressed in matrix form as

$$\mathbb{W} \widehat{\boldsymbol{\omega}} = \mathbb{F}_\omega,$$

$$\mathbb{W} = \Delta n \int_S G_{xs} \boldsymbol{N}_\omega'^T \boldsymbol{N}_\omega' \ ds, \quad \mathbb{F}_\omega = \int_S G_{xs} \boldsymbol{N}_\omega'^T \left(\bar{r}_n \Delta n + \frac{n^2}{2} \Big|_{n_1}^{n_2} \right) ds. \tag{51}$$

The resulting system of equations is linear and can be solved by a suitable linear algebra method [39]; the solution gives the numerical warping function of the cross section.

5. Cross sectional stiffness equations

5.1. Virtual work principle

The derivation of the blade cross sectional stiffness required the definition of a virtual work of the elastic forces; the 3D version of the virtual work of the internal forces is given by

$$\delta W_i = \int_V \delta \boldsymbol{e}^T \boldsymbol{\sigma} dV. \tag{52}$$

Recalling Eqs. (34) and (43) the internal virtual work of the blade is written as

$$\delta W_i = \int_V \delta (\boldsymbol{D}_s \boldsymbol{\varepsilon})^T \boldsymbol{C} \boldsymbol{D}_s \boldsymbol{\varepsilon} \ dV \\ = \int_V \delta \boldsymbol{\varepsilon}^T \boldsymbol{D}_s^T \boldsymbol{C} \boldsymbol{D}_s \boldsymbol{\varepsilon} \ dV \tag{53}$$

Since the generalized strain vector is only a function of the running length coordinate, i.e. x the above equation can be recast in the following form

$$\delta W_i = \int_L \delta \boldsymbol{\varepsilon}^T \left(\int_A \boldsymbol{D}_s^T \boldsymbol{C} \boldsymbol{D}_s \ dA \right) \boldsymbol{\varepsilon} \ dx, \tag{54}$$

where the term in parentheses is the cross sectional stiffness:

$$\mathbb{D} = \int_A \boldsymbol{D}_s^T \boldsymbol{C} \boldsymbol{D}_s \ dA. \tag{55}$$

Its explicit form is given by

$$\mathbb{D} = \int_A \begin{bmatrix} \mathbf{1}^T & \widehat{\boldsymbol{s}}^T \\ \boldsymbol{r}^T & r_n^\omega \mathbf{1}^T \end{bmatrix} \begin{bmatrix} A_{11} & A_{13} \\ A_{13} & A_{33} \end{bmatrix} \begin{bmatrix} \mathbf{1} & \boldsymbol{r} \\ \widehat{\boldsymbol{s}} & r_n^\omega \mathbf{1} \end{bmatrix} dA. \tag{56}$$

where $r_n^\omega = r_n + \omega_s'$.

The simplicity of the last expression is remarkable; for the sake of brevity, the algebraic steps that are performed before the computational implementation are not going to be shown, but the immediate matrix algebra gives

$$\mathbb{D} = \int_A \begin{bmatrix} A_{11} \mathbf{1}^T \mathbf{1} + A_{13} \overrightarrow{\boldsymbol{s}} + A_{33} \widehat{\boldsymbol{s}}^T \widehat{\boldsymbol{s}} & A_{11} \mathbf{1}^T \boldsymbol{r} + A_{13} \left(r_n^\omega \mathbf{1}^T \mathbf{1} + \widehat{\boldsymbol{s}}^T \boldsymbol{r} \right) + A_{33} r_n^\omega \widehat{\boldsymbol{s}}^T \mathbf{1} \\ sym & \boldsymbol{r}^T \boldsymbol{r} A_{11} + A_{13} r_n^\omega \overrightarrow{\boldsymbol{r}} + A_{33} r_n^{\omega 2} \mathbf{1}^T \mathbf{1} \end{bmatrix} dA, \tag{57}$$

where $\vec{s} = \mathbf{1}^T\hat{s} + \hat{s}^T\mathbf{1}^T$. To the author knowledge, this is the first vector closed expression for the cross sectional stiffness of a thin-walled composite blade.

It must be said that most beam formulations are written seeking the individualization of each term of the stiffness matrix, but this is not convenient if a compact and clear formulation is desired. Since the stiffness terms are blocks of second-order sub-tensors, the above fully vectorial expression is very clear and easy to handle.

This sub-tensors result from the outer product of two vectors; this suggest that there are two choices to explicitly evaluate $\mathbb{D}$: a) to write the vectors in the global system and the integrate the resulting expression or b) write the vectors in the sectional frame, then integrate and finally transform the resulting tensors to find the global stiffness. The latter is extremely advantageous because vectors expressed in the sectional frame are simpler. The choice is not possible in conventional thin-walled beam formulations, this may explain why an explicit expression for the cross sectional stiffness matrix is never presented in thin-walled beam bibliography [18,20,23,36,40].

5.2. Mass and inertia tensors

For the present formulation the mass and inertia tensors are defined as [41].

$$\mathbb{M} = \int_s \int_n \rho \, dn \, ds, \quad \mathbb{J} = \int_s \int_n \tilde{r}^T\tilde{r} \, dn \, ds \tag{58}$$

The computation of the mass tensor is straightforward because the density is piece-wisely constant in the layer. This is also the case of the inertia tensor; although, it admits computation in both the sectional and global frames. Computation of the inertia tensor in the sectional frame is simpler, it gives

$$\mathbb{J}_s = \int_s \int_n \tilde{r}^T\tilde{r} \, dn \, ds = \int_s \int_n \begin{bmatrix} r_n^2 + r_s^2 & 0 & 0 \\ & r_s^2 & -r_n r_s \\ & & r_n^2 \end{bmatrix} dn \, ds \tag{59}$$

where $\tilde{r}$ is the skew symmetric matrix of the position vector $\mathbf{r}$. The transformation of the inertia tensor to the global frame gives

$$\mathbb{J} = \mathbf{Q}_s^T\mathbb{J}_s\mathbf{Q}_s \tag{60}$$

6. Numerical tests

This section shows the performance of the formulation in several practical tests. To make a detailed comparison against the most popular 1D, 2D and 3D codes, the results and tests proposed by Chen et al. [13] are used; these tests were carefully designed to compare the modeling capabilities of existing wind turbine blade cross sectional stiffness calculation codes.

All comparisons are made assuming the VABS [28] results as the baseline; this is justified by the fact that both the formulation and the implementation used by VABS are based on detailed 2D modeling of the cross section. For the sake of brevity, only minor details of the geometrical and material data of each example are presented here, the reader can refer to [13] for further information.

6.1. Circular aluminum tube

The first test is set to analyze the performance of the formulation in a very simple case, an isotropic circular aluminum tube. In order to see the role played by the thin-wall hypothesis, the test is performed for different thickness-to-diameter ratios. Table 1 presents the results for the stiffness and inertia properties obtained with PreComp, VABS, CROSTAB together with the analytic results and the results obtained with the present formulation; the data table presented by Chen et al. [13] was reproduced.

It can be seen that the present formulation gives in general better results than all 1D codes. Numerical values are very close to both the theoretic and the VABS results. Axial, bending and torsional stiffness is captured very accurately. The limit case of thickness/diameter ratio equal to 1/3 shows the excellent performance of the approach for very thick walled isotropic cross sections. The largest error is that of the torsional stiffness, which is 2%. Both translational inertia and rotary inertia are also very accurate.

6.2. Multi-layer composite pipe

This example consist on a multi-layer composite pipe with oval shape, see Fig. 4. The pipe is thick walled and anisotropic; the lamination stacking sequence is unsymmetrical and unbalanced. It must be pointed out that in Ref. [13] dimensioning of the inner and middle radiuses of the oval is incorrect; the total thickness of the cross section is 5.08 mm instead of 2.54 mm. Also, the material properties were wrongly informed, the constants used in the calculations are: $E_{11} = 141.963$ GPa, $E_{22} = E_{33} = 9.79056$ GPa, $G_{12} = G_{12} = G_{23} = 5.9984$ GPa.

Table 2 shows that the present formulation gives results very close to VABS, this is not the case for the other 1D codes, both PreComp, FAROB and CROSTAB overestimates the axial stiffness up to 70%, the flexural stiffness up to 310% and the torsional stiffness up to 440%. The maximum error of the present formulation comes from the prediction of the torsional stiffness, which is 15% lower than the result obtained with VABS; also, the extensional-torsional coupling is 14% higher than the value predicted by VABS. Because the lamination sequence and the thickness ratio are very unfavorable for the zero hoop stress assumption, this behavior is expected. Fortunately a typical wind turbine blade section does not have this type of laminate.

6.3. Isotropic blade-like section

The next example is an isotropic wing shaped section; the main idea of the test is to generate a simple blade-like section such to permit the analytical obtention of stiffness and inertia constants. The section has a circular shape in the leading edge; the upper and lower surfaces are defined by straight lines meeting each other in the trailing edge. The cross section has a constant thickness; both geometric and material details are presented in Ref. [13].

In this example, results obtained with a 3D Ansys model are included in the assessment. Table 3 shows the comparison; J_i are rotary inertia coefficients and y_m, y_t and y_{sc} are the components in the direction of $\mathbf{E}_2$ of the center of mass, the tension center and the shear center respectively.

In order to analyze the results it must be pointed out first that the results presented in Ref. [13] are suspected to be biased by the following issues:

a) The cross section used for obtaining the VABS results are presented in Ref. [42] and it can clearly be seen that the straight sides of the blade-like section have different thickness than the circular side, this is suspected to affect mainly the extension-bending coupling and thus also the shear center location. The VABS and Ansys reported values of the shear center location are 9.750×10^{-4} and 9.590×10^{-4}, the analytical value is 25 times smaller, i.e. 3.900×10^{-5}; in Ref. [13] this difference is attributed

Table 1
Cross sectional properties of a circular aluminum tube.

| t/D		Axial	Bending	Torsional	Tras Iner	Rot Iner
1/15	PreComp	5.500×10^9	2.152×10^8	1.614×10^8	2.110×10^2	8.264
	FAROB	–	2.024×10^8	1.413×10^8	1.970×10^2	–
	CROSTAB	5.138×10^9	2.014×10^8	1.227×10^8	1.971×10^2	7.726
	VABS	5.128×10^9	2.022×10^8	1.544×10^8	1.967×10^2	7.755
	Theoretic	5.137×10^9	2.024×10^8	1.533×10^8	1.970×10^2	7.763
	Present	5.136×10^9	2.020×10^8	1.519×10^8	1.970×10^2	7.750
1/5	PreComp	1.650×10^{10}	4.832×10^8	3.556×10^8	6.329×10^2	1.856×10^1
	FAROB	–	4.042×10^8	2.288×10^8	5.067×10^2	–
	CROSTAB	1.322×10^{10}	3.804×10^8	2.106×10^8	5.070×10^2	1.461×10^1
	VABS	1.318×10^{10}	4.038×10^8	3.083×10^8	5.057×10^2	1.549×10^1
	Theoretic	1.321×10^{10}	4.042×10^8	3.101×10^8	5.067×10^2	1.546×10^1
	Present	1.321×10^{10}	4.031×10^8	3.030×10^8	5.065×10^2	1.457×10^1
1/3	PreComp	2.750×10^{10}	5.936×10^8	4.115×10^8	1.055×10^2	2.280×10^1
	FAROB	–	4.586×10^8	1.839×10^8	7.037×10^2	–
	CROSTAB	1.837×10^{10}	3.669×10^8	3.309×10^8	7.046×10^2	1.411×10^1
	VABS	1.834×10^{10}	4.586×10^8	3.515×10^8	7.034×10^2	1.759×10^1
	Theoretic	1.835×10^{10}	4.587×10^8	3.519×10^8	7.037×10^2	1.759×10^1
	Present	1.834×10^{10}	4.575×10^8	3.439×10^8	7.034×10^2	1.754×10^1
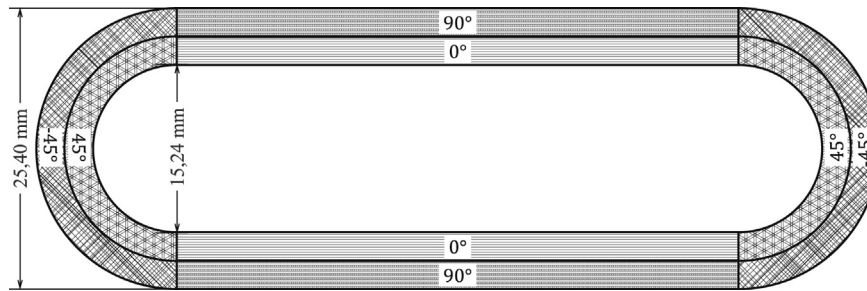
Fig. 4. Multi-layer composite pipe.

to a violation in the thin-walled hypothesis and thus the VABS results are assumed to be correct. Replicating with the present formulation the cross section used by VABS and comparing y_{sc} values obtained with the correct geometry and a geometry similar to that used in Ref. [13] it can be found that the shear center changes from 3.810×10^{-5} to 9.807×10^{-4}, this values coincide with both the analytic and the VABS results respectively. The latter observations may suggest that the discrepancies between VABS, ANSYS and the analytic results are rooted in geometric issues and not in limitations of the thin-walled approach, as stated in Ref. [13]. This point will be treated in detail in a future work.

b) The inertia tensor was very probably obtained using the center of mass as the reduction point, i.e., this affects only the J_3 value.

After considering the above comments, it is seen that results show again an excellent agreement between the present approach with VABS and Ansys. Not only the torsional stiffness is predicted with a small error, but also the extensional-torsional coupling agrees very well with VABS, Ansys and the analytical result. Both PreComp and CROSTAB are incapable of predicting this coupling

Table 2
Cross sectional properties of a multi-layer composite pipe.

	Axial	Bending 1	Bending 2	Torsional	Ext − Tors
PreComp	7.833×10^7	7.074×10^3	4.857×10^4	8.628×10^3	-1.205×10^{-2}
FAROB	–	6.182×10^3	2.297×10^4	4.240×10^3	–
CROSTAB	7.000×10^7	6.694×10^3	4.012×10^4	1.500×10^1	0.000
VABS	4.621×10^7	5.402×10^3	1.547×10^4	1.972×10^3	1.111×10^4
Present	4.588×10^7	5.370×10^3	1.539×10^4	1.722×10^3	1.269×10^4

constant correctly. Moreover both mass and inertia properties are obtained with an excellent accuracy; which is a strict requirement for modeling problems of dynamics. Precomp and CROSTAB show larger errors than the present formulation in all inertia properties.

6.4. A realistic wind turbine blade

The last example shows the performance of the present formulation in the obtention of the cross sectional properties of a realistic wind turbine blade; station 1 of the blade configuration presented in Ref. [13] is used. The material data is not presented here for brevity; the wing profile is that of an MH 104 airfoil. In this example, results presented in the work of Resor et al. [35] for specific inertia and mass properties of the cross section are included in the assessment. This results were obtained with a different version of PreComp and with BPE, a beam property extraction software based on a 3D shell finite element model of the full blade; BPE was developed by Global Energy Concepts and Sandia National Laboratories [34].

The results presented in Table 4 shows that the present approach has very good accuracy, it can be seen that it is more consistent than all the 1D software and often also than BPE. Inspecting the results of the diagonal terms of the stiffness matrix, the present approach slightly overestimates the stiffness; it is suspected that this is generated by modeling differences and not by theoretic limitations. The prediction of the torsional stiffness is remarkably good.

Regarding the coupling terms, it is observed that there are significant differences in three of the six components; since the coupling terms are very sensitive to geometric definitions it is very

Table 3
Cross sectional properties of isotropic blade-like section.

	VABS	ANSYS	PreComp	CROSTAB	Analytical	Present	Diff. VABS
Axial	3.566×10^7	3.570×10^7	3.790×10^7	3.70×10^7	3.570×10^7	3.567×10^7	0.028%
Bending 2	2.101×10^3	2.101×10^3	2.178×10^3	1.963×10^3	2.101×10^3	2.096×10^3	0.239%
Bending 3	1.050×10^4	1.051×10^4	9.100×10^3	1.153×10^4	1.110×10^4	1.112×10^4	5.900%
Torsional	1.760×10^3	1.760×10^3	1.696×10^3	1.977×10^3	1.706×10^3	1.709×10^3	2.898%
Ext-Bend	-3.046×10^5	-3.051×10^5	-3.238×10^{-2}	0.000	-3.379×10^5	-3.393×10^5	11.39%
Mass	1.843×10^{-1}	1.843×10^{-1}	1.960×10^{-1}	1.912×10^{-1}	1.843×10^{-1}	1.844×10^{-1}	0.054%
J_2	1.085×10^{-5}	1.085×10^{-5}	1.125×10^{-5}	1.014×10^{-5}	1.085×10^{-5}	1.083×10^{-5}	0.184%
J_3 (y_m)	4.080×10^{-5}	4.081×10^{-5}	4.702×10^{-5}	4.564×10^{-5}	4.081×10^{-5}	4.076×10^{-5}	0.098%
y_m	9.516×10^{-3}	9.513×10^{-3}	1.000×10^{-3}	1.045×10^{-3}	9.513×10^{-3}	9.521×10^{-3}	0.052%
y_t	9.516×10^{-3}	9.513×10^{-3}	1.000×10^{-3}	1.045×10^{-3}	9.513×10^{-3}	9.521×10^{-3}	0.052%
y_{sc}	9.750×10^{-4}	9.590×10^{-4}	1.000×10^{-2}	—	3.900×10^{-5}	3.810×10^{-5}	—

Table 4
Cross sectional properties of realistic wind turbine blade.

	PreComp [13]	PreComp [35]	CROSTAB [13]	BPE [35]	VABS [13]	Present	Diff. VABS
Axial	3.000×10^9	2.939×10^9	2.789×10^9	2.755×10^9	2.387×10^9	2475×10^9	3.68%
Bending 2	2.103×10^7	2.521×10^7	1.459×10^8	2.212×10^7	1.916×10^7	2.246×10^7	17.2%
Bending 3	6.309×10^8	4.672×10^8	4.878×10^8	4.468×10^8	4.398×10^8	4.627×10^8	5.20%
Torsional	1.008×10^7	1.389×10^7	2.469×10^7	1.572×10^7	2.167×10^7	2.160×10^7	0.32%
Bend−Bend	-8.132×10^6	—	6.010×10^7	—	1.210×10^7	2.161×10^7	78.6%
Ext-Bend	-1.037×10^6	—	5.216×10^8	—	-2.635×10^7	-7.323×10^7	178%
Ext-Bend	-1.301×10^8	—	1.685×10^8	—	-4.724×10^8	-4.727×10^8	0.06%
Bend-Tors	8.746×10^6	—	-1.208×10^9	—	1.422×10^6	1.156×10^7	713%
Ext-Tors	7.522×10^5	—	-1.723×10^9	—	-3.381×10^7	-2.793×10^7	17.4%
Mass	285.90	288.3	289.13	284.69	258.05	257.50	0.19%
J_2	2.211	2.474	5.144	3.633	2.172	2.375	9.34%
J_3	62.72	58.04	61.34	57.96	46.42	52.62	13.4%
y_m	0.332	0.402	0.284	0.403	0.278	0.398	43.2%
z_m	0.027	—	−0.028	—	0.027	0.027	0.00%
y_t	0.331	0.386	−0.029	0.267	0.233	0.198	15.0%
z_t	0.028	—	0.227	—	0.029	0.082	182%
y_{sc}	0.287	—	—	—	0.310	0.281	9.35%
z_{sc}	0.028	—	—	—	0.040	0.042	5.00%

likely that such differences are mostly originated by geometric modeling inconsistencies. Inspecting the figures that show the cross section used as VABS input in Refs. [13] and [35] it can be seen that they do not agree very well; also, they do not exactly agree with the geometric specifications in Table VI of [13]. For the sake of shortness, this issues are not analyzed here; however, it is planned to investigate in future work the accuracy of the coupling terms using exactly matching geometries.

Regarding the inertia characteristics of the blade, the present approach gives again the most accurate results. The remarkable precision in modeling the section mass is of extreme importance for dynamics; while the present approach gives an error of 0.2%, the best of the other approaches gives an error of 10%. The same tendency is obtained for the inertia terms J_i. The present approach gives a large z_t component, an explanation of this difference is to be found.

It must be pointed out that there are some differences between the results presented in Table VIII of [13] and the stiffness matrix there presented. Also, the material properties used for Nexus are wrongly informed.

7. Conclusions

Computing the cross sectional stiffness and inertia properties of realistic composite blades with a one dimensional discrete approach based on the classical lamination theory and numerical warping was proven to be a very effective approach.

Assuming a large deformation-small strain scenario, which is typical of large composite blades, permits to obtain an extremely simple and compact expression for the 6x6 stiffness and inertia matrices. This is greatly helped by the simplification of the constitutive equations of the composite laminate at the layer level; then invocation of the plane stress hypothesis gives a 2x2 layer constitutive matrix.

The simplifications introduced at the kinematic and constitutive levels do not generate an observable reduction in accuracy; moreover, the capability of the formulation to be embedded in multibody algorithms is not altered.

It is possible to obtain an analytic expression for every stiffness and inertia coefficient in terms of second order sub-tensors. The use of a vectorial formulation also permits the integration in the sectional frame of the stiffness and inertia matrix expressions, which greatly simplifies the expressions of the sub-tensors.

Several benchmark tests showed that the presented approach gives very good results. In general, it gives better results than the 1D codes: FAROB, PreComp and CROSTAB. The diagonal terms of the stiffness matrix show better agreement than the off-diagonal terms; the obtained inertia matrix is always very accurate. The off diagonal terms are in general not presented in the literature, but it is very probable that a very close agreement between the approaches would not be found. The off diagonal terms are very sensitive to geometrical modelling, so a detailed comparison between the 1D and 2D would require a very strict agreement between the models.

Although a more exhaustive comparison should be conducted, preliminary results suggest that the formulation could give at least equal results than the 3D shell code BPE. Future works shall be oriented to benchmark the formulation using cross sections for

which strict geometric definitions, material mapping and experimental results are available.

Acknowledgments

References

[1] UpWind. Design limits and solutions for very large wind turbines. 2011. p. 108. http://www.upwind.eu/.
[2] Spera DA. Wind turbine Technology. New York: ASME; 2009.
[3] Jonkman JM, Butterfield S, Musial W, Scott G. Definition of a 5-MW reference wind turbine for offshore system development. National Renewable Energy Laboratory; 2009.
[4] Hansen MOL. Aerodynamics of wind turbines. London: Earthscan Publications Ltd; 2008.
[5] Hansen MOL, Sørensen JN, Voutsinas S, Sørensen N, Madsen HA. State of the art in wind turbine aerodynamics and aeroelasticity. Prog Aerosp Sci 2006;42: 285—330.
[6] Hau E. Wind turbines. 2nd ed. Berlin: Springer; 2006.
[7] Saravia CM, Machado SP, Cortínez VH. A composite beam finite element for multibody dynamics: application to large wind turbine modelling. Eng Estruct 2013;56:1164—76.
[8] Chen J, Wang Q, Shen WZ, Pang X, Li S, Guo X. Structural optimization study of composite wind turbine blade. Mater Des 2013;46:247—55.
[9] Griffith DT, Ashwill TD. The Sandia 100-meter all-glass baseline wind turbine blade: SNL100—00. Sandia National Laboratories; 2011.
[10] Buhl ML, Andreas M. A comparison of wind turbine aeroelastic codes used for certification. National Renewable Energy Laboratory; 2006.
[11] Larsen TJ, Hansen AM, Buhl T. Aeroelastic effects of large blade deflections for wind turbines. D.U.o. Technology. In: Proceeding of the science of making torque from wind, The Netherlands; 2004. p. 238—46.
[12] Buhl ML, Wrigth AD, Pierce KG. Wind tubine design codes: a comparison of the structural response. NREL; 2000.
[13] Chen H, Yu W, Capellaro M. A critical assessment of computer tools for calculating composite wind turbine blade properties. Wind Energy 2010;13: 497—516.
[14] Saravia CM, Machado SP, Cortínez VH. A composite beam finite element for multibody dynamics: application to large wind turbine modeling. Eng Struct 2013;56:1164—76.
[15] Hodges DH. Nonlinear composite beam theory. Virginia: American Institute of Aeronautics and Astronautics, Inc; 2006.
[16] Hodges DH, Yu W. A rigorous, engineer-friendly approach for modelling realistic, composite rotor blades. Wind Energy 2007;10:179—93.
[17] Cortínez VH, Piovan MT. Vibration and buckling of composite thin-walled beams with shear deformability. J Sound Vib 2002:701—23.
[18] Fraternali F, Feo L. On a moderate rotation theory of thin-walled composite beams. Compos Part B Eng 2000;31:141—58.
[19] Gonçalves R, Ritto-Corrêa M, Camotim D. A large displacement and finite rotation thin-walled beam formulation including cross-section deformation. Comput Methods Appl Mech Eng 2010;199:1627—43.
[20] Librescu L. Thin-walled composite beams. Dordrecht: Springer; 2006.
[21] Machado SP, Cortínez VH. Non-linear model for stability of thin-walled composite beams with shear deformation. Thin Walled Struct 2005;43: 1615—45.
[22] Pi YL, Bradford MA. Effects of approximations in analyses of beams of open thin-walled cross-section—part II: 3-D non-linear behaviour. Int J Numer Methods Eng 2001;51:773—90.
[23] Piovan MT, Cortínez VH. Mechanics of thin-walled curved beams made of composite materials, allowing for shear deformability. Thin Walled Struct 2007;45:759—89.
[24] Saravia CM, Machado SP, Cortínez VH. A geometrically exact nonlinear finite element for composite closed section thin-walled beams. Comput Struct 2011;89:2337—51.
[25] Yu W, Hodges DH, Volovoi VV, Fuchs ED. A generalized Vlasov theory for composite beams. Thin Walled Struct 2005;43:1493—511.
[26] Wang L, Liu X, Guo L, Renevier N, Stables M. A mathematical model for calculating cross-sectional properties of modern wind turbine composite blades. Renew Energy 2014;64:52—60.
[27] Laird DL. NuMAD User's manual. Sandia National Laboratories; 2001.
[28] Cesnik CES, Hodges DH. VABS: a new concept for composite rotor blade cross-sectional modeling. J Am Helicopter Soc 1997;42:27—38.
[29] Yu W, Volovoi VV, Hodges DH, Hong X. Validation of the variational asymthotic beam sectional analysis. IAA J 2002;40:2105—13.
[30] Philippidis TP, Vassilopoulos AP, Katopis KP, Voutsinas SG. A software for fatigue design and analysis of composite rotor blades. Wind Eng 1996;20: 349—62.
[31] Bir G. User's guide to PreComp. National Renewable Energy Laboratory; 2005.. In: http://wind.nrel.gov/designcodes/preprocessors/precomp/PreComp.pdf.
[32] Lindenburg C. STABLAD. Stability analysis tool for anisotropic rotor blade panels. Energy Research Center of the Netherlands; 2008.
[33] Resor B, Paquette J, Laird DL, Griffith DT. An evaluation of wind turbine blade cross section analysis techniques. In: 18th structural dynamics and materials conference. Orlando, Florida: American Institute of Aeronautics and Astronautics; 2010.
[34] Malcolm DJ, Laird DL. Extraction of equivalent beam properties from blade models. Wind Energy 2007;10:135—57.
[35] Resor B, Paquette J. Uncertainties in prediction of wind turbine blade flutter. In: Structural dynamics and materials conference. Denver, Colorado: American Institute of Aeronautics and Astronautics; 2011.
[36] Barbero E. Introduction to composite material design. London: Taylor and Francis; 2008.
[37] Jones RM. Mechanics of composite materials. London: Taylor & Francis; 1999.
[38] Saravia MC. A large deformation-small strain formulation for the mechanics of geometrically exact thin walled beams. Thin-Walled Struct 2014;84:443—51.
[39] Zienkiewicz OC, Taylor RL. The finite element method. Oxford: Buttherworth-Heinemann; 2000.
[40] Vlasov VZ. Thin-walled elastic beams. 2nd ed. Jerusalem, Israel: Israel Program for Science Translation; 1961.
[41] Saravia MC, Machado SP, Cortínez VH. A consistent total Lagrangian finite element for composite closed section thin walled beams. Thin-Walled Struct 2012;52:102—16.
[42] Hu T. A validation and vomparison about VABS-IDE and VABS-GUI. Utah State University; 2012. All Graduate Plan B and other Reports. Paper 334, http://digitalcommons.usu.edu/gradreports/334.